

Supplementary Information

Facile preparation of loess-coated membranes for multifunctional surfactant-stabilized oil-in-water emulsion separation

Xiaoyang Wang^a, Mouji Li^a, Yongqian Shen^{*,b}, Yaoxia Yang^a, Hua Feng^a, Jian Li^{*,a}

a Research Center of Gansu Military and Civilian Integration Advanced Structural Materials, College of Chemistry and Chemical Engineering, Northwest Normal University, Lanzhou 730070, P. R. China.

b State Key Laboratory of Advanced Processing and Recycling of Non-ferrous Metals, Key Laboratory of Nonferrous Metal alloys and Processing, Ministry of Education, School of Materials Science & Engineering, Lanzhou University of Technology, Lanzhou 730050, China.

Corresponding author email: jianli83@126.com; syqch@163.com

Supplementary figures

Fig. S1. The cross-sectional image of the original PVDF membrane.

Fig. S2. The particle size distribution of the loess pretreated with HCl solution.

Fig. S3. Pore size distribution and average pore size of the loess-coated PVDF membrane.

Fig. S4. AFM image of the original PVDF membrane surface.

Fig. S5. EDS spectra of the loess-coated PVDF membrane.

Fig. S6. XRD patterns of the acidifying loess powders.

Fig. S7. The FT-IR spectra of the sodium alginate.

Fig. S8. (a) Photograph of the loess-coated PVDF membrane. (b) The vacuum driven filtration system.

Fig. S9. Optical microscope images, photographs, and droplet size of different stabilized emulsions and filtrates. (a) diesel-in-water emulsion, (b) hexane-in-water emulsion, (c) heptane-in-water emulsion and (d) petroleum ether-in-water emulsion.

Fig. S10. The water flux of the pure PVDF and loess-coated PVDF membrane.

Fig. S11. The oil content in water of hexane-in-water emulsion after 10 separation cycles.

Fig. S12. The permeation flux of the loess-coated membrane for cyclic separation experiments containing permeation fluxes of water and surfactant-stabilized hexane-in-water emulsion.

Fig. S13. The digital images of the kerosene-in-water emulsion before and after one-time separation by the original PVDF membrane (the middle vial) and the loess-

coated membrane (the right vial).

Fig. S14. The sodium alginate bonding mechanism with the loess.

Fig. S15. Optical microscope images and droplet size distributions of the feed and filtrate for (a) kerosene-in-NaCl, (b) kerosene-in-NaOH, (c) crude-in-NaCl, (d) crude-in-NaOH corrosive emulsions.

Fig. S16. The FE-SEM images of loess-coated PVDF membrane after separation of (a) kerosene-in-Water, (b) kerosene-in-NaCl, (c) kerosene-in-HCl, and (d) kerosene-in-NaOH emulsions, respectively.

Fig. S17. The photographs of dyes at different concentrations and the loess-coated membrane before and after dye adsorption.

Fig. S18. The EDS spectra of the loess-coated PVDF membranes after the adsorption of (a) Cu^{2+} , (b) Pb^{2+} and (c) Zn^{2+} , respectively.

Movie S1. The video of separating kerosene-in-water emulsion using the loess-coated PVDF membrane.

Movie S2. The video of separating kerosene-in-water emulsion using the pure PVDF membrane.

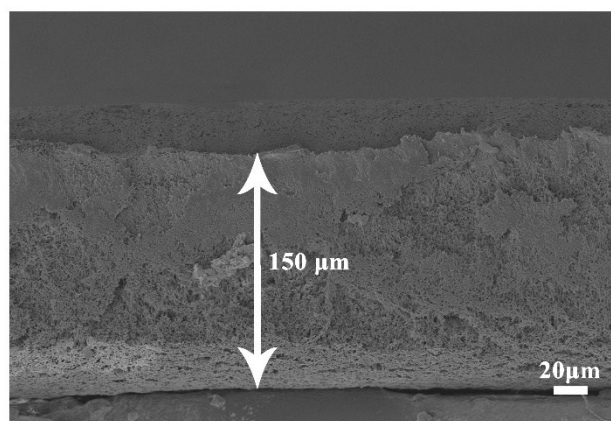


Fig. S1. The cross-sectional image of the original PVDF membrane.

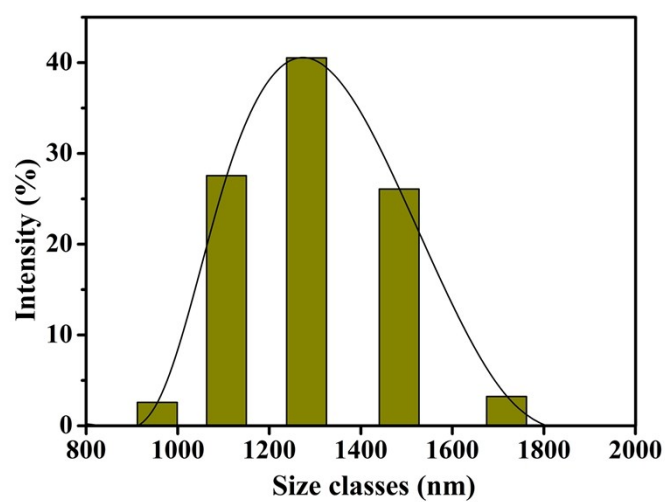


Fig. S2. The particle size distribution of the loess pretreated with HCl solution.

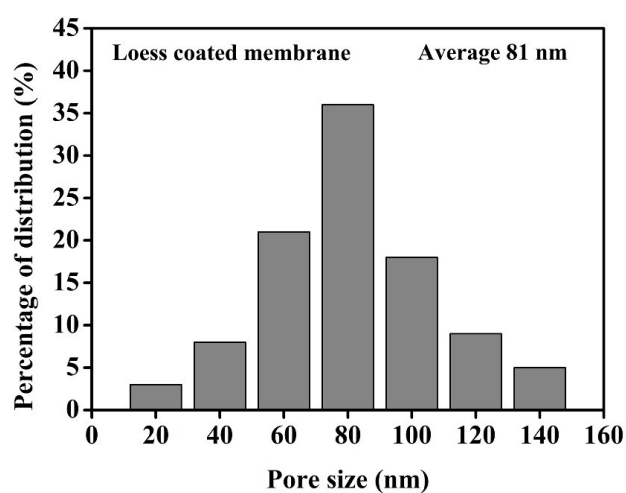


Fig. S3. Pore size distribution and average pore size of the loess-coated PVDF membrane.

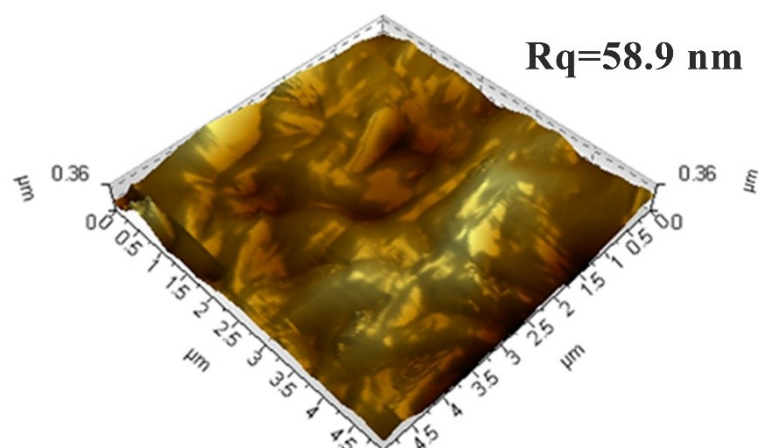


Fig. S4. AFM image of the original PVDF membrane surface.

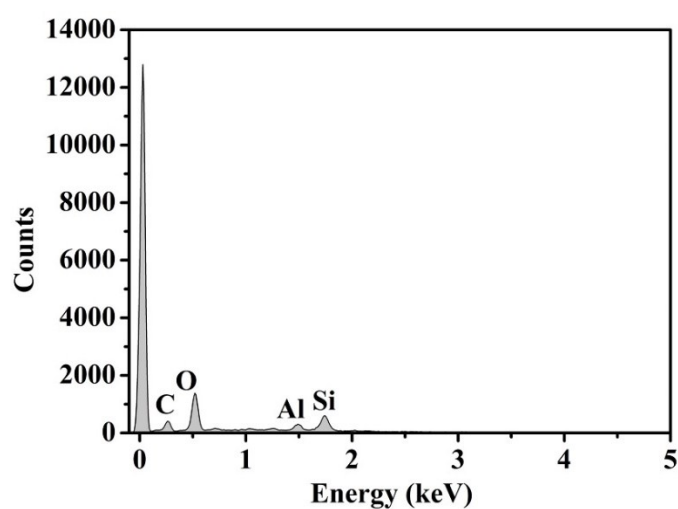


Fig. S5. EDS spectra of the loess-coated PVDF membrane.

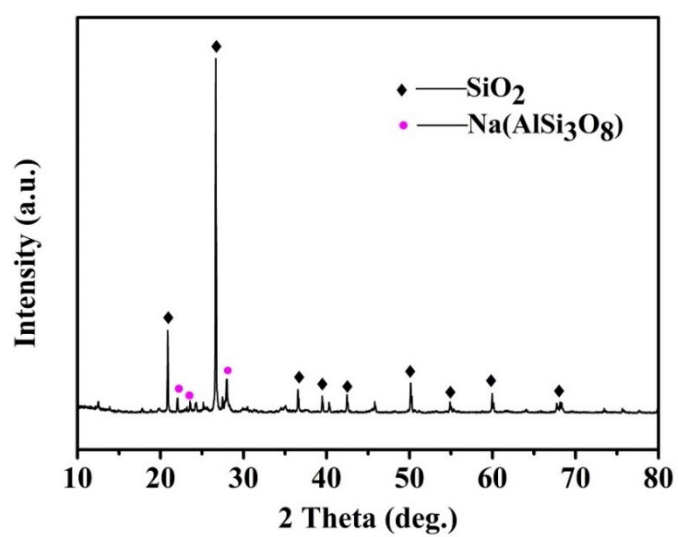


Fig. S6. XRD patterns of the acidified loess powders.

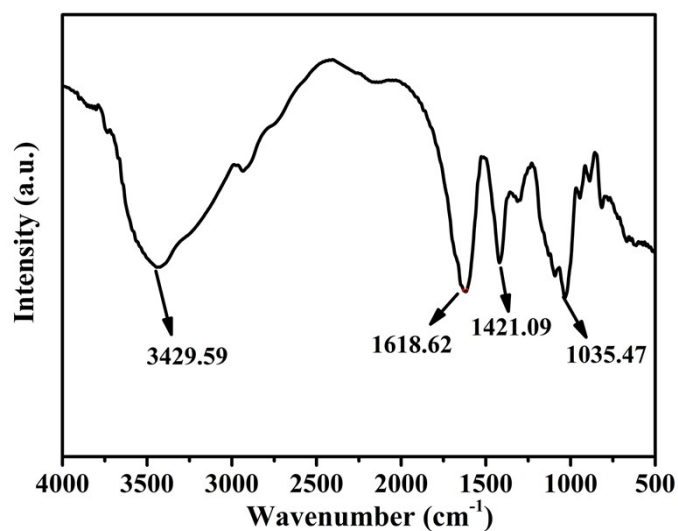


Fig. S7. The FT-IR spectra of the sodium alginate.

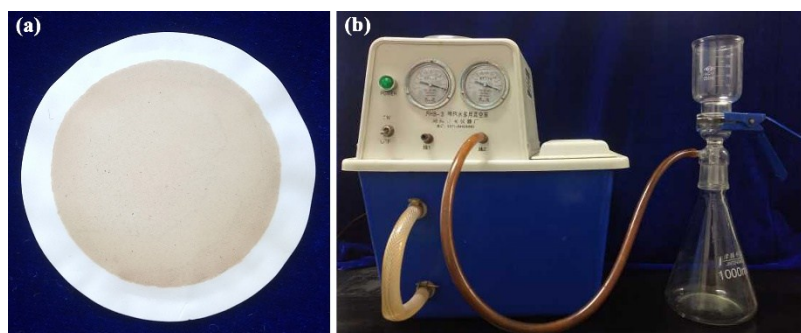


Fig. S8. (a) Photograph of the loess-coated PVDF membrane. (b) The vacuum driven filtration system.

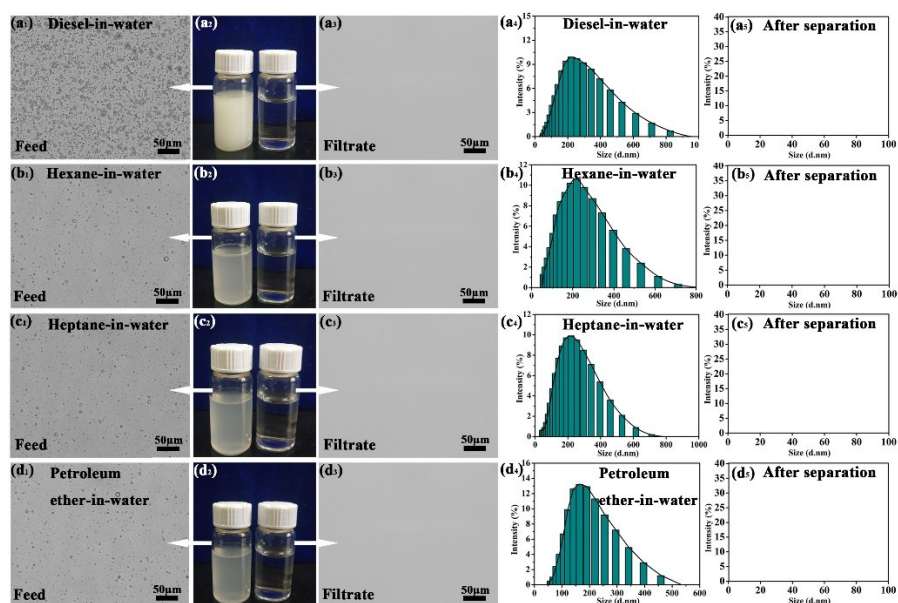


Fig. S9. Optical microscope images, photographs, and droplet size of different stabilized emulsions and filtrates. (a) diesel-in-water emulsion, (b) hexane-in-water emulsion, (c) heptane-in-water emulsion and (d) petroleum ether-in-water emulsion.

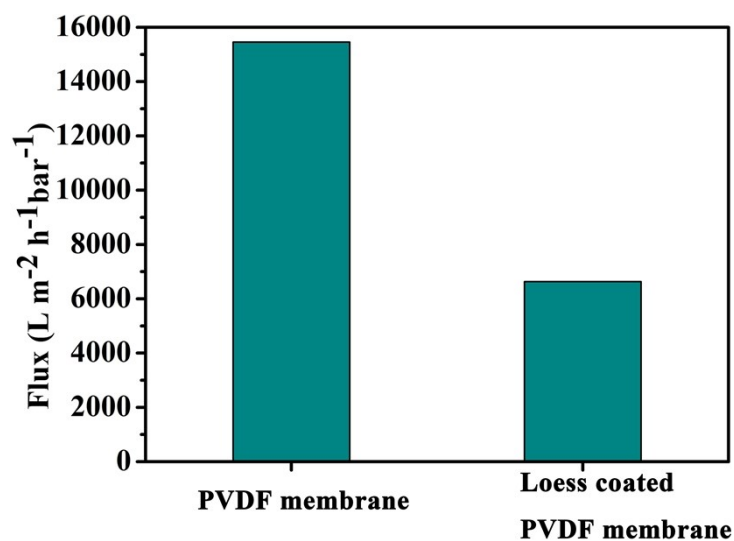


Fig. S10. The water flux of the pure PVDF and loess-coated PVDF membrane.

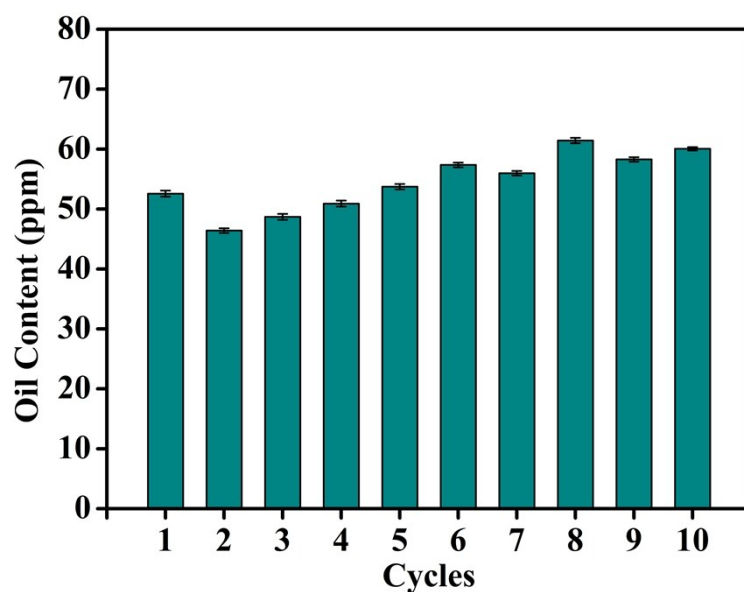


Fig. S11. The oil content in water of hexane-in-water emulsion after 10 separation cycles.

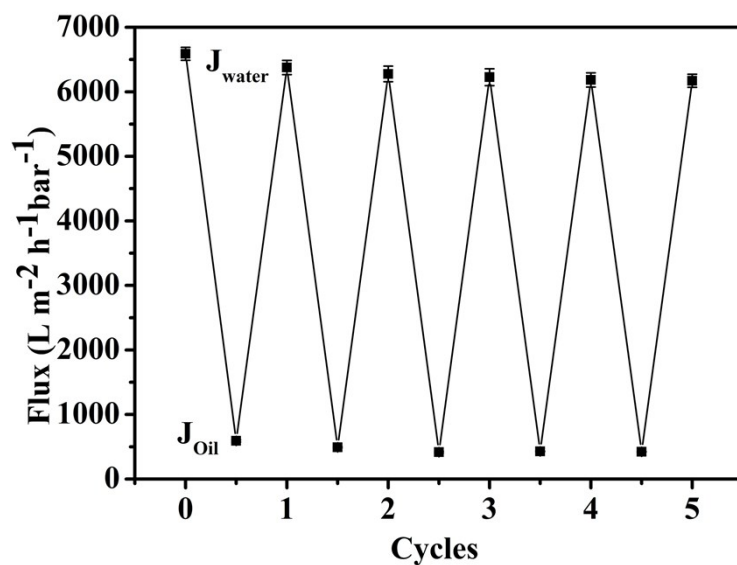


Fig. S12. The permeation flux of the loess-coated membrane for cyclic separation experiments containing permeation fluxes of water and surfactant-stabilized hexane-in-water emulsion.



Fig. S13. The digital images of the kerosene-in-water emulsion before and after one-time separation by the original PVDF membrane (the middle vial) and the loess-coated membrane (the right vial).

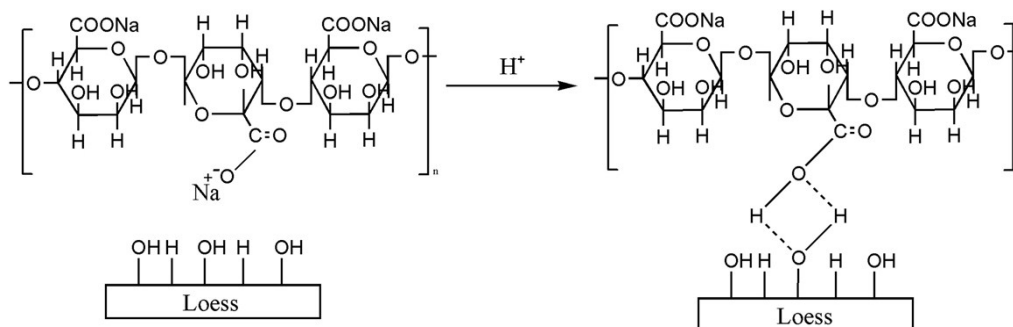


Fig. S14. The sodium alginate bonding mechanism with the loess.

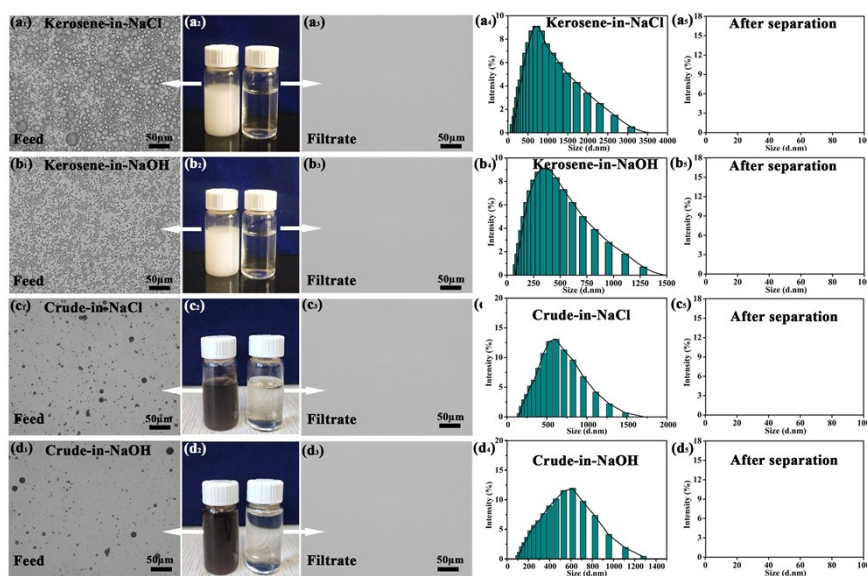


Fig. S15. Optical microscope images and droplet size distributions of the feed and filtrate for (a) kerosene-in-NaCl, (b) kerosene-in-NaOH, (c) crude-in-NaCl, (d) crude-in-NaOH corrosive emulsions.

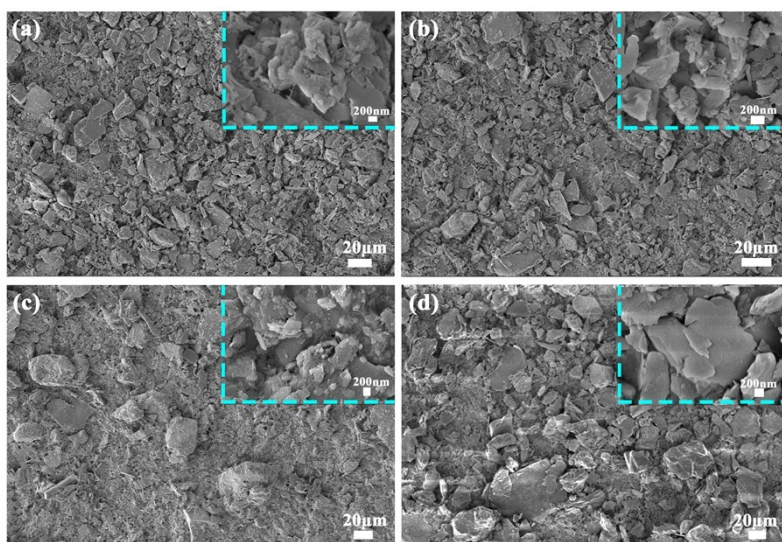


Fig. S16. The FE-SEM images of loess-coated PVDF membrane after separation of (a) kerosene-in-Water, (b) kerosene-in-NaCl, (c) kerosene-in-HCl, and (d) kerosene-in-NaOH emulsions, respectively.

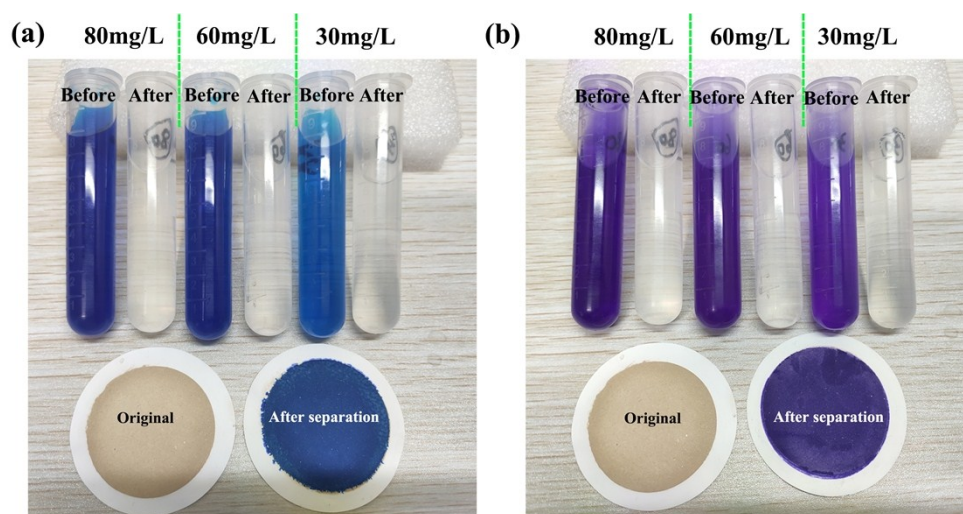


Fig. S17. The photographs of dyes at different concentrations and the loess-coated membrane before and after dye adsorption.

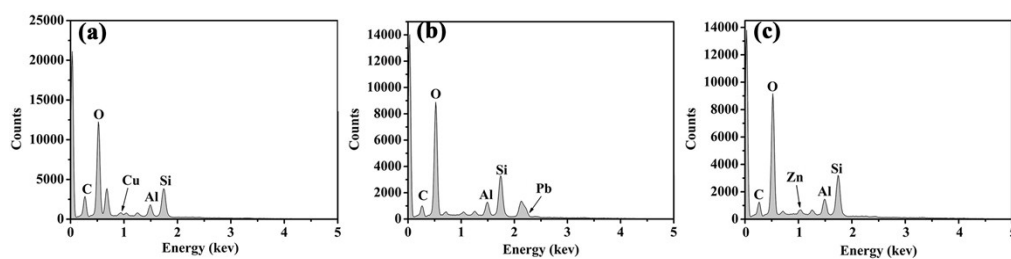


Fig. S18. The EDS spectra of the loess-coated PVDF membranes after the adsorption of (a) Cu^{2+} , (b) Pb^{2+} and (c) Zn^{2+} , respectively.